Nonlocal Magnetic Field-Tuned Quantum Criticality in Cubic $CeIn_{3-x}Sn_x$ ($x = 0.25$)

A. V. Silhanek,[1] Takao Ebihara,[2] N. Harrison,[1] M. Jaime,[1] Koji Tezuka,[2] V. Fanelli,[1] and C. D. Batista[1]

[1]*National High Magnetic Field Laboratory, Los Alamos National Laboratory, MS E536, Los Alamos, New Mexico 87545, USA*

[2]*Department of Physics, Shizuoka University, Shizuoka 422-8529, Japan*

(Received 13 December 2005; revised manuscript received 27 February 2006; published 23 May 2006)

We show that antiferromagnetism in lightly ($\approx 8\%$) Sn-doped $CeIn_3$ terminates at a critical field $\mu_0 H_c = 42 \pm 2$ T. Electrical transport and thermodynamic measurements reveal the effective mass m^* not to diverge, suggesting that cubic $CeIn_3$ is representative of a critical spin-density wave (SDW) scenario, unlike the local quantum critical points reported in anisotropic systems such as $CeCu_{6-x}Au_x$ and $YbRh_2Si_{2-x}Ge_x$. The existence of a maximum in m^* at a lower field $\mu_0 H_x = 30 \pm 1$ T may be interpreted as a field-induced crossover from local moment to SDW behavior as the Néel temperature falls below the Fermi temperature.

DOI: 10.1103/PhysRevLett.96.206401 PACS numbers: 75.30.Fv, 71.10.Hf, 71.27.+a, 73.43.Nq

When the Néel temperature T_N of an antiferromagnet is tuned to absolute zero at a quantum critical point (QCP), the uncertainty principle leads to a divergence in the characteristic length scale of the fluctuations of the staggered-moment order parameter Ψ [1]. In itinerant d- or f-electron antiferromagnets, strong on-site correlations often cause the renormalized Fermi temperature T^* to become comparable to T_N. A potential locally critical scenario arises in which the extent to which the d or f electrons *locally* contribute charge degrees of freedom to the Fermi liquid becomes subject to fluctuations at the QCP [2,3]. Their effective localization is conditional upon the inequality $T_N > T^*$ being satisfied [4], necessitating $T^* \rightarrow 0$ at the QCP as depicted in Fig. 1(a). Several f-electron antiferromagnets, including $CeCu_{6-x}Au_x$ [3,5], $YbRh_2Si_{2-x}Ge_x$ [6], and $CeRhIn_5$ [7], appear to provide examples of such behavior as function of pressure p, magnetic field H, or chemical substitution x. However, no experiment has yet been able to gauge the extent to which local criticality requires the spin fluctuations to be two-dimensional (2D) [2,3]. Were this an absolute prerequisite, the three-dimensional (3D) spin fluctuation spectrum of cubic $CeIn_3$ should then provide the essential f-electron counterexample to local criticality [2,8]. One should then expect a quantum critical spin-density wave (SDW) scenario to prevail [9] in which T^* remains finite at the QCP as depicted in Fig. 1(b).

In spite of $CeIn_3$ being one of the two original f-electron antiferromagnets in which non-Fermi liquid behavior and superconductivity were reported together under pressure [10], the comparatively large Néel temperature ($T_N \approx 10$ K) requires rather extreme experimental conditions for its complete suppression; i.e., the critical pressure is $p_c \approx 25$ kbar while the critical magnetic field is $\mu_0 H_c \approx 61$ T [11]. Neither the steep gradient $\partial T_N/\partial p$ near p_c [10] nor the pulsed magnetic fields required to access H_c are amenable to precision tuning of the temperature dependent electrical resistivity $\rho(T)$ or direct measurements of the specific heat $C_p(T)$. Prior studies [10,12,13] had therefore been unable to determine the applicable scheme in Fig. 1.

In this Letter, we utilize the fact that Sn substitution of only $\sim 8\%$ of the In sites in $CeIn_3$ (yielding $CeIn_{2.75}Sn_{0.25}$) reduces T_N to ≈ 6.4 K [14,15], enabling quantum criticality of the same type II antiferromagnetic phase as in pure $CeIn_3$ to be tuned by static magnetic fields $\mu_0 H \leq 45$ T. This also avoids technical difficulties associated with performing $C_p(T)$ and uniform magnetization $M_z(H)$ measurements in combined high pressure, strong magnetic field conditions. Sn modifies the electronic structure by reducing the separation between the Fermi energy and the core $4f$-electron level, pushing this system towards mixed valence [16]. Prior measurements on single crystalline $CeIn_3$ had shown $T_N(H)$ to be independent of the orientation of H, enabling the use of polycrystalline samples.

Polycrystalline $CeIn_{3-x}Sn_x$ buttons with $0 < x < 0.75$ are prepared by arc melting the appropriate quantities of 99.9, 99.999 and 99.9999% pure Ce, Sn, and In, respectively, with 5 further arc melts performed after flipping the button between melts for the purposes of homogenization. Samples cut from this button have $\rho(T)$ and $C_p(T)$ reproducing those of Pedrazzini *et al.* [14]. *In situ* $C_p(T)$ and $\rho(T)$ measurements on characterized samples are then extended to 45 T.

Figure 2 shows the T, H phase diagram of $CeIn_{2.75}Sn_{0.25}$ extracted from the raw $C_p(T)/T$ and $\rho(T)$ data presented in Figs. 3(a) and 3(b). The transition at T_N corresponds to a

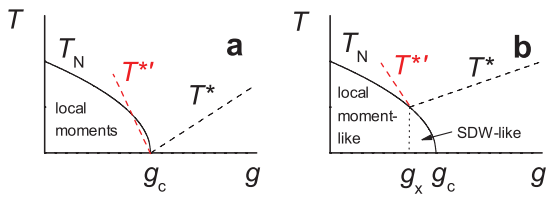

FIG. 1 (color). Temperature scale schematic of antiferromagnetic quantum criticality tuned at $g = g_c$ according to (a) the locally critical scenario and (b) the SDW scenario. The dotted line at g_x in (b) separates regions where the antiferromagnetism is predominantly local momentlike and SDW-like. The parameter g may correspond to p, H, or x.

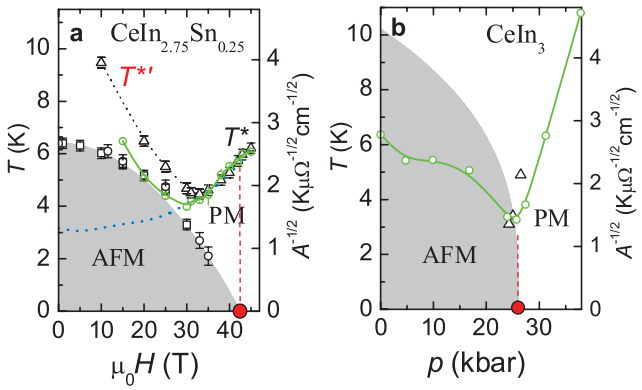

FIG. 2 (color). (a) T, H phase diagram of $CeIn_{2.75}Sn_{0.25}$ extracted from $C_p(T)$ (○ symbols) and $\rho(T)$ data (□ symbols) as described in the text. Grey shaded regions represent the antiferromagnetic (AFM) phase under the fitted $T_N = T_{N,0}(1 - (H/H_c)^2)$ curve. △ symbols delineate maxima in $\partial\rho/\partial T$ which approximately delineate the Fermi temperature T^* in the paramagnetic region. Green circles show the fitted $A^{-1/2}$ values for $n = 2$ and $T \ll T^*$. The red dashed line represents H_c, while the blue dotted line is $1/\chi' = \partial H/\partial M$ approximately determined from $M_z(H)$ after smoothing and rescaling. All other lines are spline fits between data points. (b) The equivalent phase diagram versus p using the available data of Knebel *et al.* [12]. Here the △ symbols represent T^* of Kawasaki *et al.* [13].

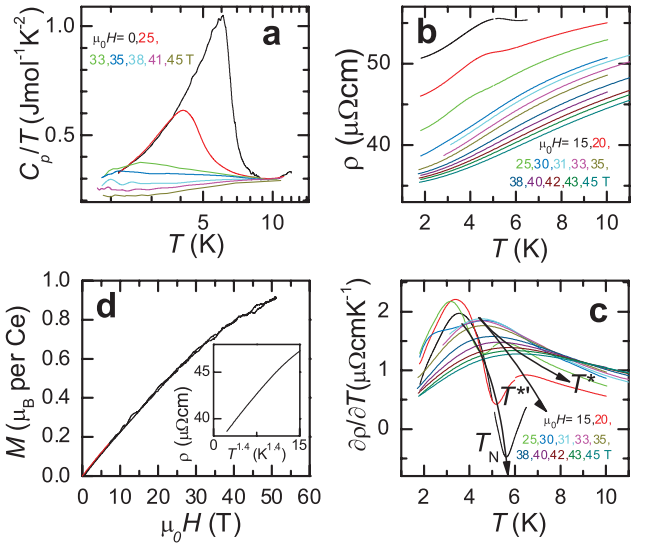

FIG. 3 (color). (a) $C_p(T)/T$ raw data at selected magnetic fields H. (b) $\rho(T)$ data at selected magnetic fields. (c) The differential resistivity $\partial\rho(T)/\partial T$ obtained after polynomial smoothing the raw $\rho(T)$ data. (d) Magnetization of $CeIn_{2.75}Sn_{0.75}$ at 450 mK. The inset shows $\rho(T)$ at 30 T plotted versus $T^{1.4}$.

minimum in $\partial(C_p(T)/T)/\partial T$ (○ symbols), which can be further identified with a minimum in $\partial\rho(T)/\partial T$ (□ symbols) in Fig. 3(c) for $\mu_0 H \lesssim 30$ T. An empirical fit of $T_N = T_{N,0}(1 - (H/H_c)^2)$ to the ○ and □ data points in Fig. 2(a) yields $\mu_0 H_c = 42 \pm 2$ T. The presence of an anomaly in $C_p(T)/T$ at 35 T and its absence at 45 T are consistent with this estimate for H_c. Several factors reveal the transition to remain of 2nd order as $H \to H_c$. These include the vanishing magnitude of the anomaly in $C_p(T)/T$ in Fig. 3(a), the absence of a jump in $M_z(H)$ at 450 mK in Fig. 3(d) and the comparatively shallow slope $\partial T_N/\partial H$ of the phase boundary in Fig. 2 such that $H_c \partial T_N/\partial H \ll p_c \partial T_N/\partial p$ [11].

The limit of $C_p(T)/T$ as $T \to 0$ provides an estimate of the extent to which electronic correlations augment $C_p(T)$. It is apparent from Fig. 3(a) that $C_p(T)/T$ does not exhibit a logarithmic divergence as $T \to 0$ at or near H_c, in stark contrast to the H-tuned QCPs of $CeCu_{6-x}Au_x$ [5] and $YbRh_2Si_{2-x}Ge_x$ [6]. The lack of divergence in $CeIn_{2.75}Sn_{0.75}$ is more consistent with the SDW scenario [9]. A similar lack of divergence occurs with $m^*(H, p)$ obtained from p- and H-dependent de Haas–van Alphen experiments on pure $CeIn_3$ for $\mathbf{H} \parallel \langle 100 \rangle$ [11,17,18]. The electrical transport measurements presented in Fig. 3(b) further support this hypothesis. $\partial\rho(T)/\partial T$ in Fig. 3(c) yields a maximum at T^* for $\mu_0 H \gtrsim 30$ T below which the curve becomes linear as $T \to 0$, consistent with Fermi liquid behavior where $\partial\rho(T)/\partial T \approx 2AT$ [19]. As expected, fits of $\rho = \rho_0 + A_n T^n$ to this data yield $n \approx 2$ in Fig. 4(a) to within ~5%, which is comparable to the experimental errors. With the exception of $\mu_0 H \approx 30$ T, fixing $n = 2$ does not change A_n by an amount significantly different from the experimental errors in Fig. 4(a), but does facilitate a comparison with other Fermi liquid parameters. $A^{-1/2} \propto 1/m^*$ can be seen to scale with T^* for $\mu_0 H \gtrsim 30$ T in Fig. 2(a), suggesting that T^* approximately corresponds to the Fermi temperature, as noted in other systems [6,20]. $A^{-1/2}(H)$ and $T^*(H)$ also scale with the inverses susceptibility $1/\chi'(H)$ for $H > H_c$, plotted in Fig. 2(a), indicating that both $\rho(T, H)$ and $M_z(H)$ are

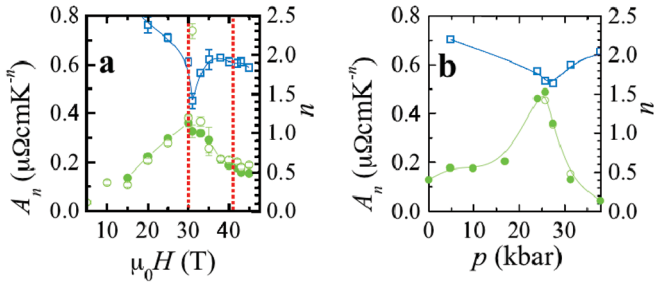

FIG. 4 (color). Coefficient A for $CeIn_{3-x}Sn_x$ estimated from $\partial\rho(T)/\partial T$. (a) shows A (filled green circles) estimated as a function of H for $x = 0.25$ and $n = 2$ with open circles showing estimates of A_n where n (open blue squares) is allowed to vary in order to facilitate a comparison with similar measurements under p. Spline fits are draw to guide the eye. An actual plot of $\rho(T)$ versus $T^{1.4}$ at 30 T is shown in the inset of Fig. 3. (b) shows similar A data for $x = 0$ as a function of p obtained by Knebel *et al.* [12].

consistent with a Fermi liquid comprised of partially polarized quasiparticle bands. While A can be seen to exhibit qualitatively similar maxima as a function of H and p [12] in Fig. 4, the plotting of $A_2^{-1/2} \propto T^*$ in Fig. 2 provides a more informative picture of how the Fermi liquid develops. Rather than vanishing at H_c and p_c, as for the local QCP [2,3] depicted in Fig. 1(a), $A^{-1/2} \propto T^* \propto 1/m^*$ can be seen to intercept both $H = H_c$ and $p = p_c$ at finite values in Figs. 2(a) and 2(b) as expected for the SDW scenario depicted in Fig. 1(b).

Taken together, the above findings imply that the quantum fluctuations of Ψ have a similarly weak effect on the Fermi liquid properties at both p_c in pure $CeIn_3$ and H_c in $CeIn_{2.75}Sn_{0.25}$. Hence, while $CeCu_{6-x}Au_x$ [3], $YbRh_2Si_{2-x}Ge_x$ [6] and $CeRhIn_5$ [7] may be considered consistent with the local criticality picture in which the Fermi surface topology undergoes a dramatic change at the QCP [3], this clearly cannot be the case for $CeIn_3$ and $CeIn_{2.75}Sn_{0.25}$.

One advantage of the present H-tuned QCP is that the slope of the phase boundary as $T_N \rightarrow 0$ in Fig. 2(a) is sufficiently gradual as a function of H that we can continue to follow the proportionality between $A_n^{-1/2}$, T^* and χ'^{-1} over a significant $\sim$12 T wide interval in field below H_c. This continues until $A^{-1/2}(H)$ (rescaled in units of kelvin) intersects $T_N(H)$. The coincidence of the minimum in $A(H)^{-1/2}$ (or maximum in A) at $\mu_0 H_x = 30 \pm 1$ T with the point on the phase diagram at which $T_N \approx T^*$ in Fig. 1(b) is strongly suggestive of its association with a crossover from SDW-like behavior to local momentlike behavior of the form depicted in Fig. 1(b). Such a crossover would directly affect the degree to which the f electrons contribute charge degrees of freedom to the Fermi liquid [4].

Outside the antiferromagnetic phase, the f electrons hybridize with the conduction electrons giving rise to heavy Fermi liquid composed of renormalized quasiparticle bands that incorporate the f-electron charge degrees of freedom [21]. On-site correlations weaken with increasing g (i.e., p or H), causing $A^{-1/2}$, T^*, and χ'^{-1} *all* to increase. Provided $T_N \ll T^*$, a weak coupling SDW that gaps parts of the Fermi surface can form [2,9] with no significant change in the overall effect of the correlations on T^*. To compute the influence of a finite antiferromagnetic order parameter Ψ on the quasiparticle bands, it is necessary to combine the effect of the on-site Kondo interaction with the $\mathbf{K} = \mathbf{Q}$ ($\mathbf{Q}$ is the antiferromagnetic wave vector) Bragg scattering produced by the underlying antiferromagnetic structure.

At the local QCP depicted in Fig. 1(a), T^* vanishes precisely at $g = g_c$ because the Kondo screening is suppressed by the magnetic interactions. The Fermi surface undergoes a large reconstruction across the QCP since the development of antiferromagnetism inhibits the f-electron contribution of charge degrees of freedom to the Fermi liquid [2,3], possibly leading to the emergence of new Fermi liquid with a different (smaller) Fermi surface topology and a different characteristic $T^{*\prime}$ that now increases with decreasing g [6] [depicted in red in Fig. 1(a)]. In the quantum critical SDW scenario depicted in Fig. 1(b), however, the Kondo screening is not suppressed at the QCP and the Fermi surface evolves smoothly across the phase transition.

The experimental $\partial\rho(T)/\partial T$ data yield two maxima for $\mu_0 H \lesssim 30$ T. The upper maximum (i.e., $T > T_N$) evolves continuously from that observed at higher H, but starts to increase again at low H (or low g). Since T_N exceeds the minimum value of T^* on decreasing H or p, the f-electron charge degrees of freedom become decoupled from the Fermi liquid. We therefore attribute the upper maximum in $\partial\rho(T)/\partial T$ to the modified Fermi temperature $T^{*\prime}$ associated with the gradual loss of correlations, as depicted in Fig. 1(b). The loss in proportionality between $T^{*\prime}$ and $A^{-1/2}$ for $H < H_x$ nevertheless reveals difficulties with characterizing the Fermi liquid for $H < H_x$. Owing to its close proximity to T_N, the determination of $T^{*\prime}$ may become subject to systematic error for $H \ll H_c$, while magnon scattering [10] causes n to deviate upward from that expected for a Fermi liquid in Figs. 4(a) and 4(b). Actual values of A_2 should therefore be considered somewhat tentative for $H \ll H_c$ and $p \ll p_c$. The estimated $T^{*\prime}$ at $\approx$ 10 T is nevertheless comparable to $T_F^* \approx \varepsilon_F/3k_B$ estimated as the approximate temperature where significant thermal depopulation occurs for the heaviest de Haas–van Alphen (dHvA) orbits that dominate the thermodynamic mass of pure $CeIn_3$ [22]. Here, $\varepsilon_F = \hbar eF/m^*$ is the effective Fermi energy for a given dHvA frequency F.

It is clearly evident from Fig. 2(a) that $H_x \neq H_c$. This can be demonstrated in the present study because $H_c \partial T_N/\partial H \ll p_c \partial T_N/\partial p$ close to the QCP. More finely p-tuned nuclear quadrupole resonance studies [13] have recently shown that the lowest Fermi liquid temperature (equivalent to T^*) occurs at a pressure that is ≈ 0.75 kbar lower than p_c, suggesting also that $p_x \neq p_c$. This observation combined with the similar values of $A^{-1/2}(n = 2)$ at which $A^{-1/2}(H, p) \propto T^*(H, p)$ intercepts T_N suggests that the p- and H-dependent QCP's are related. Similarities are also found in the p- and H-dependent fitted values of n and A_n when n is left as a free parameter in Fig. 4. Both p and H lead to a gradual reduction in the size of the staggered moment and monotonic increase in T^* as the effect of the on-site correlations is suppressed. In the former case this is caused by an increase overlap between the f-electron orbitals while in the latter case it is caused by the progressive polarization of the f electrons by the Zeeman interaction.

The monotonic $M_z(H)$ of $CeIn_{3-x}Sn_x$ in Fig. 3(d) is another quality that can be attributed to its cubic symmetry. Magnetically anisotropic systems, by contrast, sometimes undergo abrupt increases in M_z (i.e., metamagnetism) at a

characteristic magnetic field H_m that is unrelated to antiferromagnetism [23]. Systems that combine both antiferromagnetism and metamagnetism tend to exhibit a more complicated H-dependent behavior. $CeRh_2Si_2$ [24] and UPd_2Al_3 [25] are two examples of systems in which metamagnetism causes antiferromagnetism to terminate prematurely at H_m owing to the fact that M_z and Ψ compete for the same spin degrees of freedom.

In summary, we find that the light Sn doping of $CeIn_3$ facilitates observation of a H-tuned QCP at $H_c = 42 \pm 2$ T, enabling $\rho(T)$ and $C_p(T)$ measurements to be performed in static magnetic fields $\mu_0 H < 45$ T. Neither $A^{-1/2}$, T^* nor χ'^{-1} collapse to zero at the QCP, nor does n deviate significantly from $n = 2$, indicating that the system continues to exhibit conventional Fermi liquid behavior as $T_N \rightarrow 0$, suggestive of a 3D quantum critical SDW scenario as opposed to a locally critical scenario. We attribute the observation of a minimum in T^* and $A^{-1/2}$ at a somewhat lower field $H_x = 30 \pm 1$ T to the fact that the Kondo screening is not suppressed at the QCP. Correspondingly, T^* decreases until it intersects the antiferromagnetic phase boundary ($T^* = T_N$). At that point, T^*, now $T^{*\prime}$, starts to increase because T_N becomes larger when the magnetic field is reduced Fig. 1(b). A larger T_N leads to a weaker effective Kondo coupling between the f and the conduction electrons. Similarities in the electrical transport behavior of $CeIn_{2.75}Sn_{0.25}$ at $H_x < H_c$ and $CeIn_3$ at $p_x < p_c$ [13] suggests that a similar QCP may be accessed in both cases.

The possible universality in the H and p dependence warrants further $\rho(T)$ investigations of pure $CeIn_3$ under combined high H and p conditions. Realization of a situation in which the maximum in m^* and antiferromagnetic QCP occur at distinctly different pressures in $CeIn_3$ [i.e., $p_x \neq p_c$ in Fig. 1(b)] [13] may provide an opportunity to identify the key factors required to optimize unconventional superconductivity [10]. The present separation between H_x and H_c, enables us to infer that $n \sim 1.5$ is associated with g_x rather than the QCP at g_c.

This work was performed under the auspices of the National Science Foundation, the Department of Energy (US), the State of Florida and the Grant-in-Aid Scientific Research on Priority Areas 'High Field Spin Science in 100T' from MEXT (Japan). T. E. thanks the Suzuki and CASIO foundations for support, and Dr. Kitazawa of NIMS for providing his furnace. A. V. S. acknowledges Pablo Pedrazzini for useful discussions, while V. F. thanks the NHMFL In-House Research Program.

[1] S. Sachdev, *Quantum Phase Transitions* (Cambridge University Press, Cambridge, 1999).
[2] P. Coleman *et al.*, J. Phys. Condens. Matter **13**, R723 (2001).
[3] Q. Si *et al.*, Nature (London) **413**, 804 (2001).
[4] In the local quantum critical picture, the magnetic interactions suppress the Kondo screening and, correspondingly, the coherence temperature T^* vanishes at the QCP. Since the RKKY mediated antiferromagnetic order competes with the Kondo screening responsible for formation of the heavy Fermi liquid, it is unlikely that a heavy Fermi liquid that includes the f-electron charge degrees of freedom can continue to survive inside the antiferromagnetic phase. Decoupling of the f-electron charge degrees of freedom from the Fermi liquid should eventually lead to local moment ordering and development of a weakly correlated Fermi liquid with a higher Fermi temperature.
[5] A. Schröder *et al.*, Phys. Rev. Lett. **80**, 5623 (1998); O. Stockert *et al.*, Phys. Rev. Lett. **80**, 5627 (1998); K. Heuser *et al.*, Phys. Rev. B **57**, R4198 (1998).
[6] J. Custers *et al.*, Nature (London) **424**, 524 (2003); S. Paschen *et al.*, Nature (London) **432**, 881 (2004).
[7] p-dependent dHvA studies on $CeRhIn_5$ reveal m^* to exhibit a pronounced maximum and the Fermi surface topology to gain ≈ 1 f electron on suppressing antiferromagnetism with p, both of which are consistent with a local QCP; H. Shishido *et al.*, J. Phys. Soc. Jpn. **74**, 1103 (2005).
[8] J. Lawrence and S. M. Shapiro, Phys. Rev. B **22**, 4379 (1980).
[9] T. Moriya, Phys. Rev. Lett. **24**, 1433 (1970); J. A. Hertz, Phys. Rev. B **14**, 1165 (1976); A. J. Millis, Phys. Rev. B **48**, 7183 (1993).
[10] N. D. Mathur *et al.*, Nature (London) **394**, 39 (1998).
[11] T. Ebihara *et al.*, Phys. Rev. Lett. **93**, 246401 (2004).
[12] G. Knebel *et al.*, Phys. Rev. B **65**, 024425 (2002).
[13] S. Kawasaki *et al.*, J. Phys. Soc. Jpn. **73**, 1647 (2004).
[14] P. Pedrazzini *et al.*, Physica (Amsterdam) **312–313B**, 406 (2002).
[15] An unidentified phase appears for $x \gtrsim 0.3$, possibly involving an x-induced closure of the gap between the Γ_7 and Γ_8 crystal electric field levels [14].
[16] J. Lawrence, Phys. Rev. B **20**, 3770 (1979).
[17] M. Endo *et al.*, Phys. Rev. Lett. **93**, 247003 (2004).
[18] H orientation-dependent dHvA experiments performed on pure $CeIn_3$ at ambient pressure inside the antiferromagnetic phase indicate that m^* increases as $H \rightarrow H_c$ at "hot spots" that occupy $\lesssim 2\%$ of the spherical d-sheet Fermi surface area [11], possibly contributing to the H and p dependences of A inside the AFM phase in Fig. 2.
[19] K. Kadowaki and S. Woods, Solid State Commun. **58**, 507 (1986).
[20] K. H. Kim *et al.*, Phys. Rev. Lett. **91**, 256401 (2003); K. H. Kim *et al.*, Phys. Rev. Lett. **93**, 206401 (2004).
[21] A. C. Hewson, *The Kondo Problem to Heavy Fermions* (Cambridge University Press, Cambridge, England, 1993).
[22] M. Endo, N. Kimura, and H. Aoki, J. Phys. Soc. Jpn. **74**, 3295 (2005).
[23] J. Flouquet *et al.*, Physica (Amsterdam) **319B**, 251 (2002).
[24] At ambient pressure, metamagnetism at H_c coincides with H_m, while under high pressures, metamagnetism occurs in the absence of magnetic ordering; T. Hamamoto *et al.*, Physica (Amsterdam) **281–282B**, 64 (2000).
[25] T. Terashima *et al.*, Phys. Rev. B **55**, R13369 (1997).